

# On the sources of fast and slow solar wind

U. Feldman<sup>1</sup> and E. Landi<sup>1</sup>

E. O. Hulbert Center for Space Research, Naval Research Laboratory, Washington, D. C., USA

N. A. Schwadron

Southwest Research Institute, San Antonio, Texas, USA

Received 24 November 2004; revised 14 April 2005; accepted 6 May 2005; published 30 July 2005.

[1] The slow speed solar wind as measured at the Earth orbit and beyond is characterized by its velocity of  $\simeq 400 \text{ km s}^{-1}$ , by its coronal composition and by its frozen-in temperature (from carbon charge-states) of  $1.4\text{--}1.6 \times 10^6 \text{ K}$ . In contrast the fast speed solar wind is characterized by its velocity of  $\simeq 750 \text{ km s}^{-1}$ , its nearly photospheric composition and its frozen-in temperature of  $\simeq 8 \times 10^5 \text{ K}$ . The solar wind is believed to originate very close to the solar surface, but since it is accelerated significantly above the solar surface, its velocity cannot be correlated with remote observations to trace its origin. In contrast, elemental abundances and freeze-in temperatures can be used as tracers for locating the sources from which the slow and fast solar winds emerge. By comparing remote observations with properties of the solar wind observed in situ, the most likely structures from which solar wind plasmas emerge can be identified. In the present paper we review the current understanding of the morphological features present in the solar upper atmosphere and their physical properties such as electron temperature, electron density and elemental abundances. In addition, we discuss these observations in the context of recent theories describing the emergence of new magnetic flux to power the solar wind, and more traditional models that treat the background field and solar wind as a steady phenomenon.

**Citation:** Feldman, U., E. Landi, and N. A. Schwadron (2005), On the sources of fast and slow solar wind, *J. Geophys. Res.*, **110**, A07109, doi:10.1029/2004JA010918.

## 1. Introduction

[2] At Sunspot minimum, when the solar surface is devoid of active regions, the solar atmosphere consists of coronal holes covering primarily the poles, and quiet regions covering the rest of the surface area. During solar minimum, the solar wind is composed by a fast ( $\simeq 750 \text{ km s}^{-1}$ ) and a slow component ( $\simeq 400 \text{ km s}^{-1}$ ); traditionally the former is associated with the high heliographic latitudes and the latter with the mid-latitudes surrounding the streamer belts [e.g., Phillips *et al.*, 1995]. Recently, Woo and Habbal [2000] argued that the traditionally strict association of the fast solar wind with the open magnetic field regions of coronal holes needs to be revised. Based on radio occultation and white light measurements of path-integrated density as well as flow speed that were inferred from Doppler dimming of the O VI lines observed by the UVCS on SOHO they concluded that fast wind originates from both the quiet Sun and polar coronal hole regions.

[3] The composition in the two wind types is distinctly different: in slow speed wind, elements having low first

ionization potential (FIP  $\leq 10 \text{ eV}$  - i.e. low-FIP elements) are enhanced by a factor of 3–4 relative to the photosphere, while in the fast speed their abundances are nearly photospheric [Geiss *et al.*, 1995; Zurbuchen *et al.*, 1999; von Steiger *et al.*, 2000]. Additionally, in the slow solar wind the freeze-in temperature from carbon charge-states is on the order of  $1.4\text{--}1.6 \times 10^6 \text{ K}$  and in the fast wind it is  $8 \times 10^5 \text{ K}$ . An important objective of the Solar and Heliospheric communities is to fully understand the mechanisms driving the solar wind, and in doing so, identify the sources of solar wind in the low solar atmosphere. The solar wind accelerates as it moves away from the solar surface, so particle velocities close to the solar surface, i.e. below  $1.5 R_{\text{sun}}$ , are too small to unambiguously be used to identify the sources in the inner corona from which the fast and slow wind emerge. On the contrary, frozen-in temperatures and elemental compositions, which can be measured with accuracy close to the solar surface from remote-sensing instruments, appear to be better tracers for locating sources from which the slow and the fast solar winds emerge. The importance of the properties of the plasma and magnetic field close to the solar surface has been demonstrated by Woo *et al.* [2004]: by studying the elemental composition of both the lower corona and solar wind, they showed that closed magnetic field structures close to the Sun play an important role in solar wind flow; Woo *et al.* [2004] also

<sup>1</sup>Also at Artep Inc., Ellicott City, Maryland, USA.

underline the importance of connecting low-altitude measurements of the physical properties of the corona with in situ measurements and models.

[4] The aim of the present paper is to review observations on the morphology and plasma properties of the solar upper atmosphere (SUA) close to the Sun's surface in order to provide the solar wind community with an overview of the most up-to-date results on the physical properties of the region where the solar wind is likely to be accelerated. Using observations from high resolution solar imagers and spectrometers taken since 1996, we also speculate on the structures from which solar wind plasmas emerge. In the present work, we will mostly make use of recent (1997–2004) results from SOHO/SUMER. Results from SOHO observations taken in earlier dates were reviewed by Feldman [1998]; in the present work we will extend the Feldman [1998] review and will also focus on the consequences of element abundances as well as plasma temperatures and densities on the solar wind models. Given its wide spectral coverage and extended observations of the Sun, SOHO and in particular SUMER observations have allowed a more accurate and comprehensive study of the physical properties of the solar corona than previously done. SUMER observations have been carried out systematically over nearly an entire solar cycle on solar plasmas in all physical conditions, thus allowing a more complete and accurate sampling of their physical properties than ever before; coupling of SUMER, CDS, EIT and UVCS data has allowed to place diagnostic results in a more complete context [i.e., *Teriaca et al.*, 2003].

[5] The morphology of the SUA at different temperature regimes is described in section 2. In section 3, we outline the temperature and composition properties of the SUA. Section 4 summarizes our main results, and in section 5, we present conclusions regarding the sources of the solar wind. The assumptions made and approach taken in many theoretical wind models concerning solar wind sources are discussed in section 6.

## 2. Morphology and Temperatures of Quiet Sun (QS) and Coronal Hole (CH) Structures

[6] In the 1960s and early 1970s the consensus among solar physicists was that the SUA is a single entity composed of a  $10^4$  K chromosphere and a  $10^6$  K corona connected by a very narrow interface called "transition region". In that model the SUA was depicted as a one-dimensional entity where the temperature could be uniquely defined as a function of the solar radius at all latitudes. The temperature variation with height was predicted to be very rapid in the transition region, as shown in Figure 1 [Gabriel, 1976].

[7] In the mid 1970s, mostly as a result of the Skylab mission, images of the solar corona became available. Although the spatial and temperature resolution of the recorded images were still fairly moderate, it became apparent that during minimum periods the SUA consists of two main types of regions: coronal holes (CH) associated with open magnetic field configurations, and quiet Sun (QS) regions associated with closed field configurations. CH, typically confined to the polar-regions, at times extend as far as the equator and beyond. The apparent movement of

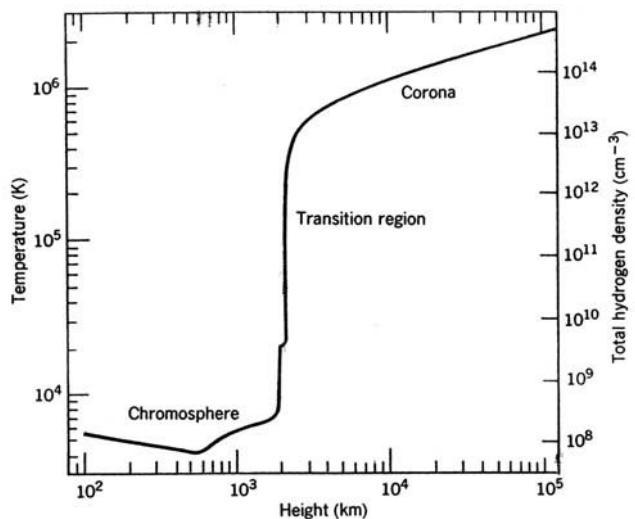


**Figure 1.** Temperature profiles for early models of the chromosphere-corona system [from *Gabriel*, 1976].

CHs across the solar visible surface and their correlation with in situ measurements of the solar wind, suggested that CHs were the source regions of the fast solar wind. QS regions were identified as the general area from which the slow speed solar wind emerges [Krieger *et al.*, 1973; Nolte *et al.*, 1977].

[8] First indications that the thin transition region models were not supported by actual SUA observations first emerged in the late 1970s and 1980s as a result of Skylab spectroscopic measurements [Feldman, 1983, 1987]. Observations made in the late 1990s by instruments aboard the Solar and Heliospheric Observatory (SOHO) [Domingo *et al.*, 1995] significantly advanced our understanding of the solar morphology. Using high spatial and temperature resolution images from Solar Ultraviolet Measurements of Emitted Radiation (SUMER) [Wilhelm *et al.*, 1995], which were recorded in narrow temperature intervals over the  $1 \times 10^4$ – $1.4 \times 10^6$  K range, and combining them with Extreme Ultraviolet Imaging Telescope (EIT) [Delaboudiniere *et al.*, 1995] and Transition Region and Coronal Explorer (TRACE) [Handy *et al.*, 1999] images at coronal temperatures ( $1\text{--}2 \times 10^6$  K), provided a new depiction of the morphology of the SUA close to the solar surface.

[9] When using radiation from low excitation lines formed at temperatures of  $T_e \leq 7 \times 10^5$  K to image the SUA, little if any morphological distinction between quiet Sun and coronal hole regions is observed. It is only when observing lines formed at coronal temperatures ( $T_e \geq 7 \times 10^5$  K) that morphological distinctions between QS and CH regions begin to emerge. As an example, Figure 2 shows a SUMER full Sun images in 977 Å C III ( $T_e \approx 7 \times 10^4$  K) and 770 Å Ne VIII ( $7 \times 10^5$  K) lines and Figure 3 presents partial Sun images in the vicinity of the southern polar region in the 1249 Å C I ( $1.3 \times 10^4$  K), 1239 Å N V ( $1.9 \times 10^5$  K), 625 Å Mg X ( $1.1 \times 10^6$  K) and 1242 Å Fe XII ( $1.4 \times 10^6$  K) lines: coronal holes are evident only in the images from coronal lines formed at or above  $7 \times 10^5$  K. For an extended review of the SUA morphology, see Feldman *et al.* [2000], and for a large collection of SUMER images, see the SOHO SUMER Atlas [Feldman *et al.*, 2003]. In what

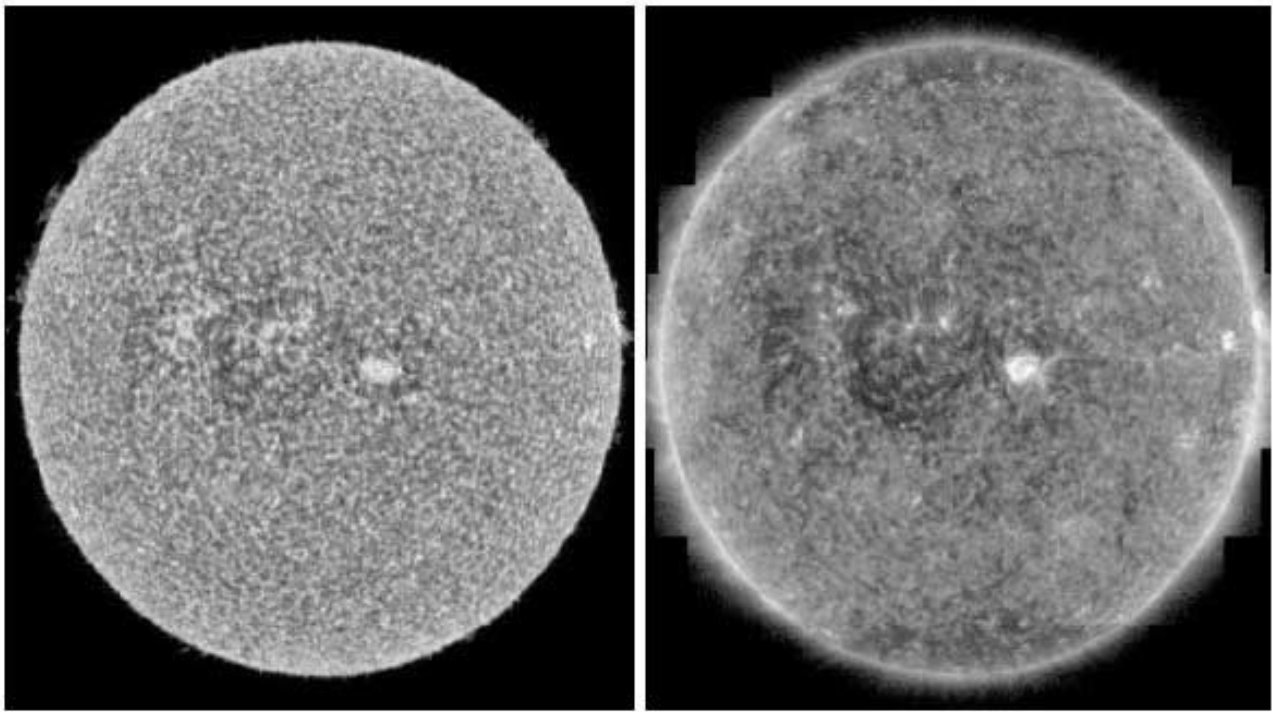


**Figure 2.** Full-Sun images in the C III 977 Å line (formed at  $T_e \simeq 7 \times 10^4$  K, left panel) and in the Ne VIII 770 Å line (formed at  $T_e \simeq 7 \times 10^5$  K, right panel).

follows, we will always discuss the electron temperature. In QS, it is usually assumed that the ion temperature and the electron temperature are equal, but in CH this is not necessarily true [Tu *et al.*, 1997].

## 2.1. The $3 \times 10^4$ – $7 \times 10^5$ K Plasma Domain

[10] The general appearances of solar fine structures with temperatures of  $3 \times 10^4$ – $7 \times 10^5$  K in QS and CH regions as seen against the solar disk are quite similar. In simultaneously recorded images practically all structures that appear at the lower temperatures also appear in the higher temperatures. The detected images are composed of bright loop-like structures located along the cell boundaries, which are 10–20 arcsec long (7000–14000 km) and have widths at or below the SUMER  $\simeq 1.5$  arcsec resolution (Figure 4). In addition fainter structures with similar lengths and widths occupy cell interiors. Small centers of emission that are not much larger than the instrument resolution elements are also visible in the image. These are the result of either small-unresolved plasma blobs that are not more than 2" in size or perhaps the bases of vertical spicule-like structures observed along their main axis. The morphology of these structures in both QS and CH structures are similar. As is already known from Skylab observations, on average, hotter structures are somewhat taller than the colder ones, and CH structures are slightly more extended than those in QS regions [Doschek *et al.*, 1976; Feldman *et al.*, 1976]. The brightness of the structures in the  $3 \times 10^4$ – $7 \times 10^5$  K range seems to change on timescales of 100–500 s.

[11] When comparing in detail an image of the SUA in lines formed at temperatures of  $T_e \leq 7 \times 10^5$  K with a simultaneously acquired image of lines formed at coronal temperatures ( $T_e \geq 7 \times 10^5$  K) practically no association

between the two is found. Clearly the colder structures are entities that are not part of the higher temperature coronal structures. The 1960s and early 1970s thin transition region model, in which the  $3 \times 10^4$ – $7 \times 10^5$  K plasmas are portrayed as a continuous interface between the chromosphere and the corona, has no observational support.

[12] In contrast to images in C III ( $T_e \simeq 7 \times 10^4$  K) and C IV ( $1.1 \times 10^5$  K) lines, images in the 304 Å line emitted by He II ( $T_e \simeq 1.0 \times 10^5$  K), clearly show the presence of coronal holes. Although both the C<sup>+3</sup> and He<sup>+</sup> ions have their maximum fractional abundance at approximately the same temperature ( $T_e \simeq 1.0 \times 10^5$  K) the excitation energy ( $\Delta E$ ) of the upper level of the C IV line is 8 eV and that of the 304 Å He II line is 41 eV. The rates of collisional excitation  $C$  to the excited levels giving rise to the observed spectral lines are proportional to the Boltzmann factor according to the equation

$$C \propto T^{-\frac{1}{2}} e^{-\frac{\Delta E}{kT}} \quad (1)$$

where  $k$  is the Boltzmann constant. The C IV excitation energy  $\Delta E$  is lower than  $kT$  at around  $1.0 \times 10^5$  K, so that small changes in the distribution of electron energies, such as an increase or decrease of the top temperature, or the presence of high-energy electrons, will have limited effects on the total excitation rate of the lines. On the contrary, the excitation energy  $\Delta E$  for He II is larger than  $kT$  so that the Boltzmann exponential factor will be strongly dependent on the electron temperature: a small decrease or increase of the plasma temperature will significantly decrease or increase the excitation rate and population of the upper level of the 304 Å line, thus changing its emitted intensity. From the above we conclude that since the He II line emission is

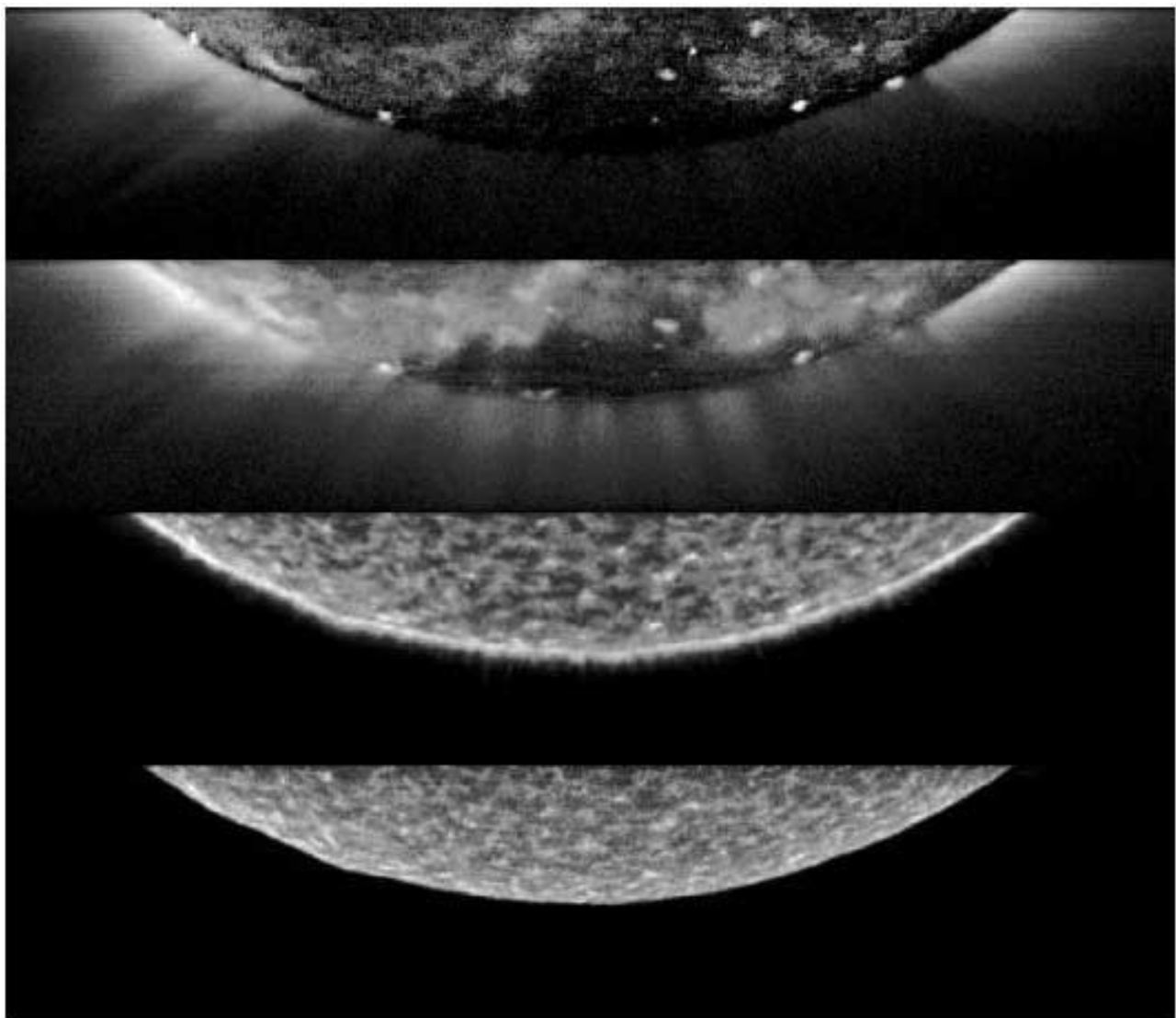


**Figure 3.** Southern polar coronal hole images observed in (from top to bottom): Fe XII ( $1.4 \times 10^6$  K - top panel); Mg X 625 Å ( $1.1 \times 10^6$  K - second panel); N V 1239 Å ( $1.9 \times 10^5$  K - third panel); and C I 1249 Å ( $1.3 \times 10^4$  K - bottom panel).

reduced in coronal hole region while the C IV line emission is approximately the same, the electrons energy distribution at  $10^5$  K in QS and CH are somewhat different, the latter being characterized by a lower temperature than the former.

## 2.2. The $7 \times 10^5$ – $1.2 \times 10^6$ K Plasma Domain

[13] The morphology of the solar upper atmosphere in the  $7 \times 10^5$ – $1.2 \times 10^6$  K range can be described from EIT and TRACE images recorded in the Fe IX/Fe X channels and in the SUMER images in the Ne VIII and Mg X lines. In the following we base the discussion on the SUMER images since they have a much greater spectral (and hence temperature) purity than EIT and TRACE images. Ne VIII and Mg X are members of the lithium isoelectronic sequence. As such, although their maximum fractional abundances is at  $6.2 \times 10^5$  K and  $1.1 \times 10^6$  K respectively, they have significant populations at much higher temperatures.

[14] The SUMER images in the Ne VIII and Mg X lines look distinctly different from the images in the colder C III and O V lines. In the colder disk images little if any differences between the QS and CH structures are present. In the Ne VIII disk image the brightness of the emission from polar CH regions is slightly lower than that from QS regions; nevertheless, coronal holes are clearly identifiable. In the hotter Mg X disk image the emissions from the CH regions are greatly reduced and only emissions from polar plume roots are bright. High resolution SUMER Ne VIII and Mg X images, as well as EIT and TRACE disk coronal images of typical quiet regions contain numerous small regions, several arcsec in size, that are similar to coronal hole regions in brightness. It is quite possible that these are a source of fast speed wind advocated by *Woo and Habbal* [2000].

[15] Above the limb, in both the Ne VIII and Mg X images, diffuse emission that appear to trace local magnetic

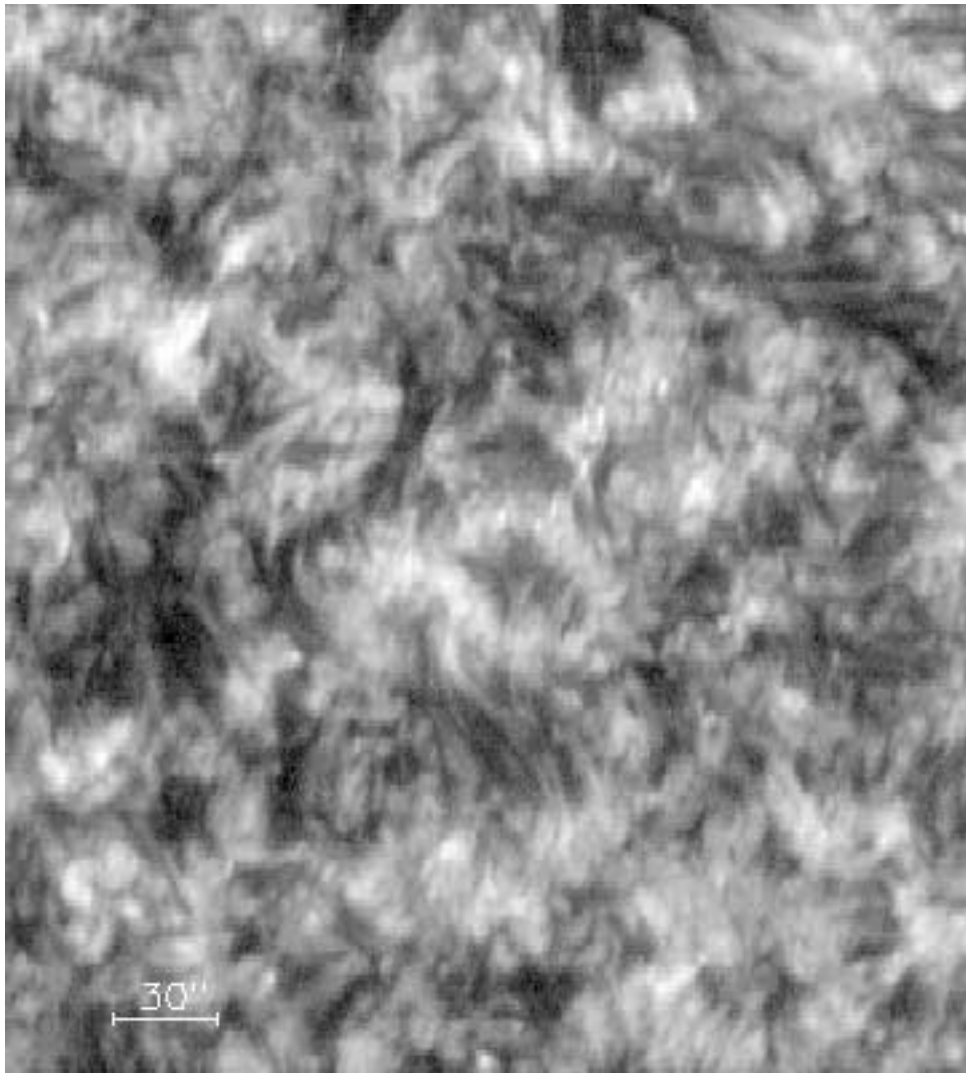


**Figure 4.** Quiet Sun observation in the O VI 1032 Å line.

fields extends to at least  $1.1 R_{\text{sun}}$  and is clearly visible above QS and CH regions (Figure 5). It appears that in QS regions there are  $(1.0 \pm 0.2) \times 10^6$  K plasmas confined in low-lying ( $h < 1.04 R_{\text{sun}}$ ) structures not present in the CH regions. The nature of these plasmas is not yet clear. In CH a large fraction of the diffuse emission is clearly associated with the long lasting (i.e., hours and possibly days) bright polar plumes. The rest arises either from fainter polar plumes, plasma in inter plume regions and/or from both. Spectroscopic [e.g., *Wilhelm*, 1999; *Young et al.*, 1999; *Dwivedi et al.*, 2000; *Doschek et al.*, 2001] and radio [e.g., *Chiuderi Drago et al.*, 1999] measurements show that the polar CH hole plasma temperature at about  $1.05 R_{\text{sun}}$  is on the order of  $(8 \pm 1) \times 10^5$  K; a few of these studies indicate that it rises to about  $(1.0 \pm 0.1) \times 10^6$  K at  $1.1\text{--}1.2 R_{\text{sun}}$ .

[16] It is important to note that spectroscopic observations of the corona above the solar limb are the sum of all the emission along the entire line of sight; thus, derived plasma properties are averaged over all the structures crossing the line of sight. When recording the coronal spectra above polar regions QS plasmas also contribute to the observed emission. Close to the solar surface, the emission of the CH

plasma is relatively high, so the foreground and background contributions are negligible since their plasmas are located at larger distances from the solar surface. However, such may not be the case at larger heights, since QS emission along the line of sight increases its importance. Based on the above, the measured increase in CH temperatures high above the limb may not be real but the result of an average between the  $8 \times 10^5$  K CH and the  $1.4 \times 10^6$  K QS coronal temperatures. The above scenario is compelling in particular because, if proven to be correct, the temperature of the CH and the fast solar wind are the same. The derived electron densities in CHs are systematically lower than those in the QS by a factor of  $\simeq 2\text{--}5$ . At a height of  $1.04 R_{\text{sun}}$  the CH density is  $\simeq 7 \times 10^7 \text{ cm}^{-3}$  and falls to about  $4 \times 10^6 \text{ cm}^{-3}$  at  $\simeq 1.3 R_{\text{sun}}$  [*Doschek et al.*, 1997]. In comparison, *Landi and Feldman* [2003] measured QS densities of about  $2 \times 10^8 \text{ cm}^{-3}$  at  $1.03 R_{\text{sun}}$ , that decreased to about  $2 \times 10^7 \text{ cm}^{-3}$  at  $1.3 R_{\text{sun}}$ .

### 2.3. The $1.2\text{--}1.6 \times 10^6$ K Plasma Domain

[17] The maximum fractional abundance of  $\text{Fe}^{+11}$  is at  $1.4 \times 10^6$  K and between  $1.2 \times 10^6$  K and  $1.6 \times 10^6$  K is

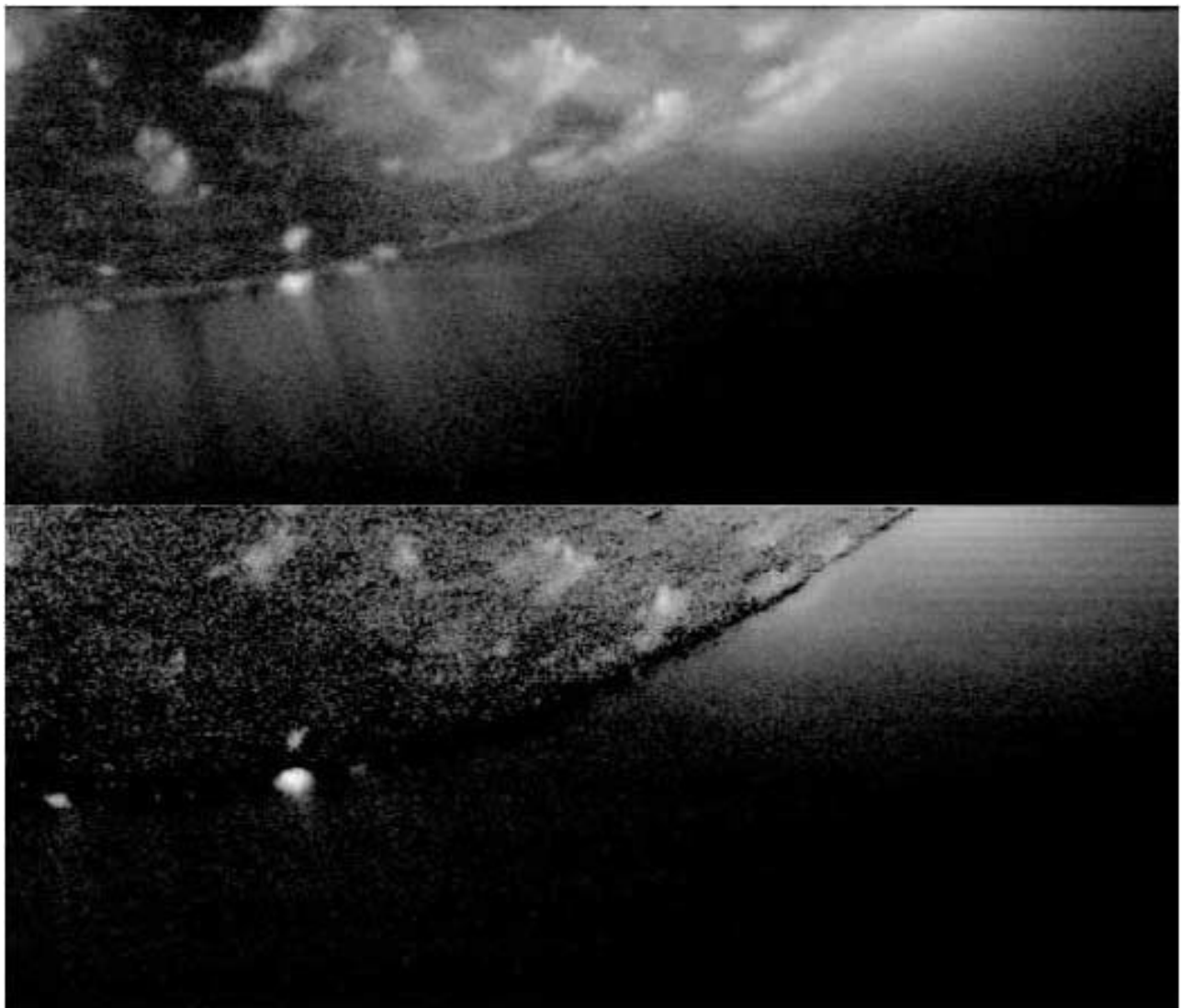


**Figure 5.** Fe XII (top) and Mg X (bottom) images of the boundary between CH and QS in the off-disk solar corona.

still within a factor of 3 from maximum. Images in the Fe XII line are distinctly different in appearance from images in Ne VIII and Mg X lines (Figure 5). No Fe XII emission appears above CH regions. As is the case with the Mg X images above QS, the Fe XII images are composed of a large number of diffuse loop-like structures. However, the Fe XII structures are more extended than the loop like structures seen in Mg X at  $T_e \simeq 1.0 \times 10^6$  K and could be perceived as a canopy that stretches above the colder loops. The  $T_e \simeq 1.4 \times 10^6$  K structures are quite stable and their average lifetimes are probably in excess of one day. Feldman et al. [1999a] applied spectroscopic techniques to probe the temperature of the diffused emission above an equatorial QS region at heights  $h = 1.03 R_{\text{sun}}$ . The minimum height was chosen in order that the colder plasmas present at even lower heights would not influence the observations. In their study, Feldman et al. [1999a] found that the coronal QS plasma at heights of  $1.03 R_{\text{sun}} \leq h \leq 1.5 R_{\text{sun}}$  is isothermal at a temperature the  $1.3 \times 10^6$  K. TRACE

movies in 195 Å Fe XII channel indicate that coronal loops are fairly stable over many hours [Feldman et al., 1999b]. Based on the above they postulated that the QS  $1.3 \times 10^6$  K plasmas are confined in closed structures that on average last a day or more.

### 3. Elemental Composition of the SUA Above QS and CH Regions

[18] Elemental composition variations in the SUA can be described by the FIP bias, defined as the factor by which the coronal abundance of an element differs from its abundance in the photosphere. Since elemental abundances are usually expressed in terms of the hydrogen abundance, the FIP bias can be expressed as

$$\text{FIP bias} = \frac{\left(\frac{N_{\text{El}}}{N_H}\right)_{\text{corona}}}{\left(\frac{N_{\text{El}}}{N_H}\right)_{\text{photosphere}}} \quad (2)$$

where  $\frac{N_{EI}}{N_H}$  is the abundance of the element (El) relative to hydrogen (H).

### 3.1. Composition of the $3 \times 10^4$ – $7 \times 10^5$ K Plasmas Above QS and CH Regions

[19] Feldman and Widing [1993] derived the elemental abundance during solar minimum in equatorial and polar limb regions at a temperature of  $\simeq 4 \times 10^5$  K by comparing intensity ratios of the high-FIP Ne VI lines with the intensities of the low-FIP Mg VI lines. According to them the elemental composition in both regions is similar to within experimental errors and stood at a FIP bias of 1.5–2.0.

### 3.2. Composition of the Diffused $7 \times 10^5$ – $1.2 \times 10^6$ K CH

[20] The elemental abundances in CH regions above the limb in polar plumes and in inter-plume regions were studied by many authors [e.g., Doschek *et al.*, 1998; Feldman *et al.*, 1998; Young *et al.*, 1999; Dwivedi *et al.*, 2000]. In both polar plume and inter-plume areas the FIP biases were found to be between 1 and 2 with uncertainties that in some cases were reported to be as large as a factor of 2. FIP bias results do not seem to vary with distance from the solar photosphere. Based on the above, we conclude that the average FIP bias in the corona above the polar CHs is 1–1.5.

### 3.3. Composition of the QS Coronal Emission in the $1.2 \times 10^6 \leq T_e \leq 1.6 \times 10^6$ K

[21] Although many observational studies of the composition of the SUA have been made in recent years, to the best of our knowledge only four extensive studies have been done of the diffuse QS corona ( $1.2 \times 10^6 \leq T_e \leq 1.6 \times 10^6$  K), and all using SUMER observations. The first of the studies was made of an isothermal ( $T_e = 1.3 \times 10^6$  K) QS region along the equatorial limb at  $1.03 R_{\text{sun}}$  [Feldman *et al.*, 1998]. Laming *et al.* [1999] made an additional study at several off-limb positions between 1.01 and  $1.10 R_{\text{sun}}$ . Both studies indicated FIP biases of 3–4 in all line ratios. Warren [1999] investigated the composition of an isothermal ( $T_e = 1.6 \times 10^6$  K) QS region above southeast limb and Widing *et al.* [2005] studied an isothermal ( $T_e = 1.4 \times 10^6$  K) QS region above the northwest limb. Both studies, which were done at  $1.05 R_{\text{sun}}$ , indicated FIP biases of 1.5–2.9.

[22] Feldman *et al.* [1998] studied the composition in the QS equatorial region as a function of distance from the solar surface. They performed the study by comparing the intensity fall-off of lines emitted by Ne, Mg and Si ions, which have similar atomic weights, with each other and with lines emitted by the twice as heavy Fe ions. In doing so, they found that over the  $1.03$ – $1.5 R_{\text{sun}}$  distance the coronal plasma was isothermal and at the same temperature. However, starting at about  $1.2 R_{\text{sun}}$  the intensities of the Fe lines began decreasing faster than lines from the lighter Ne, Mg and Si and at  $1.5 R_{\text{sun}}$  the decrease in the Fe line intensities was already twice as fast as the intensity decrease of lines from the lighter ions.

[23] It should be kept in mind that the studies reported by Feldman *et al.* [1998] and Laming *et al.* [1999] measured the composition during minimum activity and

the Warren [1999] and Widing *et al.* [2005] studies utilized observations acquired two years later during the rise of the solar cycle. Therefore differences in the FIP biases between the two sets of observations might be due either to latitudinal difference between the observations, to the solar cycle time variability, or to a combination of the two.

### 3.4. Relationship Between the Age of a Coronal Structure and Its FIP Bias

[24] In regions where the individual structures are not easily distinguishable from each other only average values of composition changes can be derived safely. However, in cases where a particular plasma structure could be isolated without ambiguity from the adjacent structures and followed in time, it is possible to estimate the rate of change of its composition. Due to the large number of structures in QS and CH regions, the only meaningful composition information that present day instruments are able to provide are average values. At present, information on the rate of change of elemental abundances in individual coronal structures is only available from long lasting active region (AR) structures that are significantly brighter than their surroundings. Not being able to directly measure the rate of abundance change in QS loops we assume that information gathered from AR structures is also applicable to QS structures. Studies show that within one to two hours after emerging from under the photosphere the FIP bias of AR structures is 1 [Sheeley, 1995; Widing, 1997]. On the other hand, the FIP bias of older AR structures could be as high as 15 [Widing and Feldman, 1992]. Realizing that the composition of loop-like structures evolves over long periods of time, Widing and Feldman [2001] studied their FIP bias rate of change from birth to decay or disappearance behind the limb. To do so, they identified bright structures very shortly after they were born and studied their spectra as they moved across the solar disk. Since it was required that the emergence of the structures occur on the visible side of the disk, the age of the flux loops under study could not exceed two weeks, i.e., the time it takes an AR born on the east solar limb to rotate all the way to the west limb. Widing and Feldman [2001] succeeded to identify half a dozen regions that met the requirements of being born on the visible side of the Sun and being detectable for at least 3 days. Using Mg VI to Ne VI intensity ratios they derived the rate of composition enrichment of small structures in the regions from the time they first become visible and until they either decayed or disappeared from view as they approach the west limb of the Sun. Figure 6 displays the derived FIP bias increase as a function of time for four of the selected regions. Widing and Feldman [2001] concluded that all the considered structures showed an increasing FIP bias with time. Immediately after emergence the bright structures show photospheric compositions, then their FIP bias value increased until they reached average coronal values (FIP bias 4) in about two days. As the structures become older and in particular after three days their FIP bias increased beyond the typical coronal value. Although the shapes of the structures in the regions studied were not identical, the rate of FIP bias increase with time was about the same in all regions. The fact that average FIP biases in QS are in

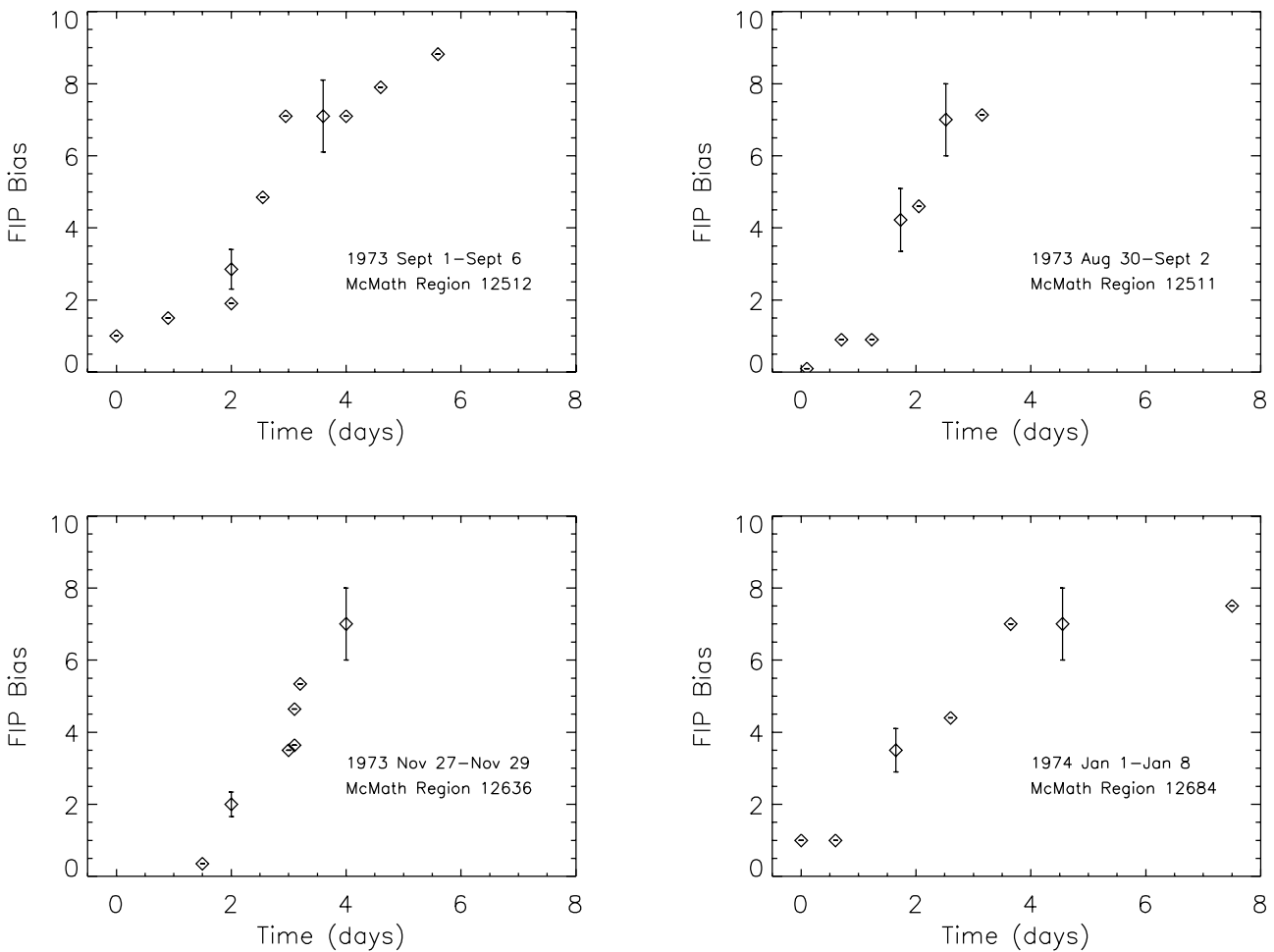


**Figure 6.** Measurements of FIP bias as a function of time in four active regions observed by Skylab [from *Widing and Feldman, 2001*].

the 2–4 range might suggest that the average lifetime of individual structures is one to two days.

#### 4. Summary of Observational Results

[25] 1. Based on morphological, temperature and composition considerations QS plasmas could be divided into three groups and the CH plasmas into two. The first group, common to both QS and CH regions, includes all plasma in the  $3 \times 10^4$ – $7 \times 10^5$  K range. The QS second group includes the  $0.7$ – $1.2 \times 10^6$  K plasmas and the QS third group the  $1.2$ – $1.6 \times 10^6$  K plasmas. The second polar CH group consists of the plasmas in the  $0.7$ – $1.1 \times 10^6$  K. These groups are listed in Table 1.

[26] 2. The plasmas in group 1, common to both QS and CH regions, are confined in filamentary structures. The diameters of the filamentary structures are on the order of 2 arcsec (1400 km) or less, and they are typically 10–20 arcsec (7000–14000 km) long. The brightness of the structures in the first group changes on timescales of 100–500 s and their FIP bias is 1.5–2.0.

[27] 3. The QS plasma in group 2 is the least explored. It appeared to have temperatures in the  $0.7$ – $1.2 \times 10^6$  K range and confined to fairly low-lying structures ( $h \leq$

$1.03 R_{\text{sun}}$ ). Due to its proximity to the solar limb and because of the difficulties separating its emission from that of the plasma in group three its composition is not yet established.

[28] 4. The QS plasma in group 3 is confined in large loops tens to hundreds of arcsecs long (up to 150000 km or more) that last for a day or two. The confined plasmas are easily detected at heights of  $1.5 R_{\text{sun}}$ , the limit of the SUMER field of view. LASCO C1 coronagraph images in the Fe XIV coronal green line (5303 Å) indicate that loop tops usually reach out to about  $1.5 R_{\text{sun}}$  and in some cases to well beyond  $2 R_{\text{sun}}$  [Schwenn *et al.*, 1997]. The plasmas of group three appear to be isothermal having temperatures of  $1.2$ – $1.6 \times 10^6$  K. At a height of  $1.04 R_{\text{sun}}$  the electron

**Table 1.** Summary of the Properties of the Structures in the Solar Upper Atmosphere

Region	T, K	FIP Bias	Lifetime	Length
1 QS, CH	$0.3$ – $7 \times 10^5$	1.5–2.0	100–500s	10–20"
2 QS	$0.7$ – $1.2 \times 10^6$			
3 QS	$1.2$ – $1.6 \times 10^6$	3–4	1–2 days	10s–100s"
4 CH	$0.7$ – $1.1 \times 10^6$	1–1.5		

density of the plasmas measured along the equatorial region is  $1.8 \times 10^8 \text{ cm}^{-3}$  and at  $1.3 R_{\text{sun}}$  it has already decreased by an order of magnitude. Starting at a height of  $1.2 R_{\text{sun}}$  elemental settling becomes apparent and at  $1.5 R_{\text{sun}}$  Fe ions are depleted by a factor of 2 when compared with Ne, Mg and Si ions. The FIP bias of the third group plasmas is 3–4.

[29] 5. The CH plasma in group 4 is clearly visible in SUMER images to heights of  $1.1 R_{\text{sun}}$  and in SUMER spectra it is detectable to at least  $1.3 R_{\text{sun}}$ . At least part of the CH plasma is confined in what is commonly called polar plumes. The temperature of the plasmas, although appear to be nearly isothermal at each height, was reported to increase slightly with distance from the limb. At  $1.05 R_{\text{sun}}$  is on the order of  $(0.8 \pm 0.1) \times 10^6 \text{ K}$  and rises to about  $(1.0 \pm 0.1) \times 10^6 \text{ K}$  at  $1.1\text{--}1.2 R_{\text{sun}}$ . As discussed in section 2.2, the increase may be the result of line of sight averaging so that the true CH temperature might be, at least below  $1.5 R_{\text{sun}}$ ,  $8 \times 10^5 \text{ K}$ . The coronal electron densities, when measured at comparable heights, are a factor 2–3 lower in CH than in the QS regions. The composition of the plasma in CH group 4 is about photospheric, i.e., FIP bias of 1–1.5.

[30] The structures from group 1 have no morphological association with the structures from the higher temperature groups. Their composition (FIP bias 1.5–2.0) is also different from the composition of the plasmas in the hotter groups. Based on morphology and composition consideration we conclude that the plasmas of the first group have no direct connection with plasmas of the hotter groups. In essence we conclude that the magnetic field keeps plasma from the first group insulated from the plasmas in the hotter groups.

## 5. Source of the Solar Wind

[31] Based on the diagnostic and morphological results reviewed above, we speculate that the slow speed wind plasma arises from plasma in the QS group 3, consisting of coronal loops close to the solar surface lasting for a day or two. This conclusion is suggested by the similarity of the temperature and composition of QS, group 3 plasma with those measured by in situ instruments. In this scenario, after the release from the confined loop-like structure, most likely as a result of the loop's disintegration, no meaningful change in composition or in ionic fractions further occurs (i.e., no additional heating of the plasma occurs as the wind accelerates).

[32] Due to elemental settling, the Fe/Mg abundance ratio decreases with height until at  $1.5 R_{\text{sun}}$  it is already a factor of 2 lower than its photospheric value. Since in the slow solar wind the Fe/Mg abundance ratio is photospheric, we conclude that most of the plasma populating the slow solar wind was originally confined for a day or two at heights smaller than  $1.2 R_{\text{sun}}$ .

[33] The origin of the fast solar wind is less obvious. Presently it is difficult to evaluate whether it arises from the polar plumes, inter-plume regions or from both. If the coronal temperature increase with distance above polar holes is real and not due to contamination from QS emission along the line of sight, the freeze-in temperature of  $8 \times 10^5 \text{ K}$  measured in the fast wind suggests that the

source of the fast solar wind plasma most likely is located at fairly low altitudes ( $h \leq 1.2 R_{\text{sun}}$ ).

## 6. Solar Wind From Loops: Theoretical Context

[34] Recent observations have yielded strong clues to the acceleration of the high-speed solar wind [Deforest *et al.*, 1997; Kohl *et al.*, 1998; Cranmer, 2002, and references therein]. The sonic point is measured via Doppler dimming to be as low as  $2 R_s$ , indicating that more than simple gas pressure balance is at play. However, there is still controversy over basic issues such as the role of polar plumes in the wind [Kohl *et al.*, 1999; Gabriel *et al.*, 2003], the location of the accelerating mechanism, the role of magnetic structure, the role of emerging magnetic flux and the sources of solar wind. The acceleration of the slow solar wind needs to be considered a dynamic, time-varying process as has been discussed by Axford [1977] and Fisk *et al.* [1999a, 1999b].

[35] The detailed profile of high and low speed solar wind acceleration depends crucially on the heating profile, and the modes of conversion between electromagnetic and hydrodynamic energy. The rapid reconfiguration of the network appears to deposit significant energy. This energy can be channeled into bulk heating and acceleration of fast solar wind through generation and subsequent dissipation of magnetohydrodynamic waves and turbulence, field braiding, and through microflaring in the network (e.g., the "furnace" model of Axford and McKenzie [1997]). It appears that a combination of these processes is required: microflaring causes localized chromospheric heating, whereas wave dissipation, braiding and turbulent heating have larger dissipation times and therefore deposit energy higher in the corona. Generally, solar wind models require both sources of heating in the chromosphere and distributed in the low corona. In this context there has been extensive work on solar wind acceleration models [Isenberg, 1989, and references therein], moment expansions of the Boltzmann equation [Olsen *et al.*, 1998; Lie-Svendsen *et al.*, 2001], multi-fluid solar wind models, and models that self-consistently damp electromagnetic waves to heat the solar wind [Hollweg, 1986; Li *et al.*, 1999]. Typically, these models have been treated in 1-D, along an individual flux tube where the area of the flux tube (which scales with the inverse of the field strength) is prescribed. There have also been some recent activities that attempt to extend aspects of the 1-D models into 2-D and 3-D [Usmanov *et al.*, 2000; Endeve *et al.*, 2003]. The 2-D models with higher order physics demonstrate the emergence of new types of complex physical behavior. As an example, Endeve *et al.* [2003] have an extended 2-D MHD model that includes electron and proton heat conduction; they find that the helmet structure can be destabilized by a reduction in the heat conduction coefficient, resulting in periodic eruptions of the streamer. This example demonstrates that models are beginning to place solar wind acceleration in the context of the global magnetic topology. Nonetheless, a detailed model capturing the relationship between global field structure, its continual re-organization, and the source of solar wind has not yet emerged. This is an active area of research, and a number of theoretical models described here have provided important insights.

[36] A challenge to any solar wind model is explaining the well organized gross features of solar wind [McComas *et al.*, 2000; *von Steiger et al.*, 2000]: the mass flux is relatively constant in both fast and slow wind; the final speed, density and other properties of fast solar wind are remarkably stable; the slow solar wind shows much larger fluctuations in all of its properties, suggesting that it can not be described as a single state; the slow solar wind shows a stronger low-FIP bias than fast wind as already discussed; and there is a remarkably robust anti-correlation between coronal freezing-in temperatures (from C and O) and the solar wind speed [Geiss *et al.*, 1995; *von Steiger et al.*, 2000; *Gloeckler et al.*, 2003].

[37] The differences between the elemental composition of fast and slow wind are particularly revealing. Elemental composition is set low down in the corona. The different elemental compositions of fast and slow wind shows that their sources are differentiated very near the solar surface. This fact is remarkable, and appears in stark opposition to traditional models with solar wind formed on steadily open magnetic field lines from coronal holes. In such models, what would cause such strong differences very low down near the solar surface? On the other hand, large differences between fast and slow solar wind may arise naturally from different source regions on the Sun. For example, fast wind may arise from coronal holes, whereas slow wind may arise from large loops beyond coronal holes. The plasma, including its elemental composition, can be quite different depending on the region (coronal hole, quiet Sun), lifetime and length of the source structure, as discussed previously. The differences in source structures would be reflected naturally in the solar wind streams they generate.

[38] The fact that fast solar wind has such stable final properties, low coronal source temperatures, and an elemental composition resembling the photosphere, immediately suggests sources from small loops or network fields that rapidly and continually re-organize open field lines. On the other hand, the larger variations in slow wind properties, the higher coronal temperatures, and larger enhancements in low-FIP ions suggests sources from large coronal loops.

[39] Coronal holes are often described as the source of the solar wind, and the Sun's open magnetic fields. However, the concept that open magnetic fields exist outside coronal holes suggests a very different picture in which open and closed magnetic fields interact to produce slow solar wind beyond coronal holes. This begs the questions of why open field lines would move outside coronal holes to begin with, and what maintains the rigid motion of coronal holes? The explanation offered by *Fisk et al.* [1999a] is that open field lines are continually dragged through the coronal hole due to the Sun's differential motion. Beyond coronal holes, to prevent the continual buildup of magnetic flux, open magnetic field lines rapidly change their position through interchange reconnection, and thereby execute large drift patterns beyond the coronal holes. The problem here of open field re-organization can be described as a form of diffusion, so-called media diffusion [*Fisk and Schwadron*, 2001], where open field lines are continually re-distributed due to reconnection with loops. In this case, the closed loops are assumed to dictate the nature of the diffusion.

Accordingly, open magnetic flux collects predominantly in regions where the diffusion by loops is least efficient for redistributing open field lines; e.g., in coronal holes. Beyond coronal holes where loops are much larger, the media diffusion is more efficient. This both causes a reduced average strength of the open magnetic flux and allows for the large scale drifts of open field lines to prevent the buildup of open magnetic flux on one side of the coronal hole. In this case, because closed loops dictate the diffusive process, the fact that coronal holes rotate rigidly at the equatorial rotation rate is a natural result of the distribution of large closed structures on the Sun.

[40] Recent remote observations due to TRACE and SOHO, including those presented here, show that the magnetic fields of the corona are in a state of continual re-organization. The network of magnetic fields in supergranules ( $\sim 20,000$  km diameter) are entirely reconfigured on time scales  $\sim 1.5$  days [e.g., *Schrijver et al.*, 1997, 1998]. Since both open and closed loops are rooted in supergranules, the open magnetic fields of the corona should also be continually re-organized. Presumably, this implies frequent reconnection between open field lines and closed loops, with the subsequent release of matter and energy from the closed onto open field lines, which may feed and power the solar wind [e.g., *Fisk et al.*, 1999b; *Fisk and Schwadron*, 2001; *Schwadron and McComas*, 2003; *Fisk*, 2003].

[41] Some large loops may act as the conduits for solar wind, temporarily storing the matter that ultimately becomes solar wind. The larger, hotter and denser the loop, the more energy fed in from supergranules is lost through radiation, and the slower the final wind speed from the large loop source [*Schwadron and McComas*, 2003]. If loops become too hot, they radiate so much energy that they cannot produce a supersonic solar wind, and would remain closed structures. Another possibility is that the larger scale heights on hot, large loops lead to increased mass on the loops, and thereby, a reduction in the final solar wind speed [*Fisk*, 2003]. In both cases, large loops are more strongly wave-heated, which may cause a stronger enhancement of low-FIP ions [*Schwadron et al.*, 1999]. Further support to the idea that loops provide the solar wind plasma is given by the variations in the speed and elemental and ionic charge composition along the solar cycle reported by *Zurbuchen et al.* [2002]. By showing that the bimodal distribution of speed and ionic charges present during solar minimum disappears during the solar maximum, while element abundances experience much less variations, *Zurbuchen et al.* [2002] argue that the theories suggesting that the solar wind originates from coronal loops reconnecting with open magnetic field lines are more consistent with with observations than theories that place the solar wind origin in coronal holes only, or that are based on the network of magnetic flux in the photosphere as the source of energy for solar wind acceleration.

[42] Although the dynamic loop source of solar wind appears to be consistent with many of the properties of solar wind observed in situ, we can not rule out the concept that the fast and slow solar wind are the result of the different expansion properties of the background solar magnetic field. *Wang and Sheeley* [2003] postulate that during periods of high solar activity two types of source regions ("1"

and “2”) exist on the solar surface. The regions are defined by: the values of the total energy flux density at the base of the corona  $F_{wo}$ ; the magnetic field  $B_0$  at the base; the expansion rate of the magnetic field  $f_{exp}$ ; and the mass conservation along a flux tube extending from the solar surface. They further postulate that the temperature steadily increases with the distance from the solar surface until it attains a maximum value  $T_{max}$ . In region 1, the temperature attains its maximum value  $T_{max}$  at a radius  $R$  that is fairly high in the corona. In region 2, where the magnetic fields are strong but fall off rapidly with distance due to the large expansion value,  $T_{max}$  occurs at a much lower height. However,  $T_{max}$  in regions 1 and 2 is expected to be fairly similar since the decrease in the local heating rate caused by the rapid areal expansion, is offset by the larger mechanical energy flux  $F_{m0}$  at the coronal base. Wang and Sheeley [2003] argue that the radius at which the coronal density falls to values low enough for the ion charge to start freezing-in is at about the height where  $T_{max}$  is reached in region 2. As a result it is expected that the freeze-in temperature emerging from region 2 will be higher than the freeze-in temperature from region 1. They also predict that since  $T_{max}(2)/R_{max}(2) \gg T_{max}(1)/R_{max}(1)$ , the downward heat flux is larger in region 2 than in region 1 and a greater enrichment in low-FIP elements occurs. Additionally they argue that most of the wind at sunspot maximum originates from small low-latitude holes characterized by large values of  $f_{exp}$ ,  $B_0$ , and hence  $F_{m0}$ . In the type 2 regions, the temperature maximum is located relatively close to the coronal base. This enhanced low-coronal heating acts to drive a greater mass flux, reduce the energy-per-proton and asymptotic wind speed, and causes a bias of low-FIP elements dragged out of the chromosphere.

[43] Woo *et al.* [2004] propose a new way of linking the chemical composition of low-altitude, closed coronal structures to the fast and slow solar wind properties. By studying the physical properties of the solar wind and of the coronal plasma, they suggest that plasma confinement time in closed magnetic structures is the key for differentiating the fast and the solar wind. Fast wind is composed by plasma confined only for a short time in closed magnetic loops, and slow wind comes from long-trapped plasma. Such differentiation explains the differences in composition between the two winds, and also explains the variations of the solar wind properties along the solar cycle, interpreting them as a stronger or weaker capability of closed magnetic structure of confining the coronal plasma in the CH area. They show that, according to the Widing and Feldman [2001] result, the elemental abundances and the FIP effect are a most effective tracer of the confinement time of the solar wind plasma, and hence a prime diagnostics of the source of the solar wind.

[44] The question remains open as to whether the ordered properties of fast and slow solar wind observed in situ reflect the coronal loop sources, or the expansion properties of the coronal magnetic field. The debate on this question is likely to continue until more definitive measurements are made of the magnetic field and solar wind in the low corona. In this paper, we have shown that there are classes of loops with compositional properties remarkably similar to those observed in solar wind. Since the elemental

composition is determined near the solar surface, the link between these classes of loops and observed solar wind states may be definitive.

[45] **Acknowledgments.** The work of Enrico Landi is supported by the NNN04AA12I and W10,232 NASA grants. Nathan S. Schwadron acknowledges financial support from the NAG512780 NASA grant. We warmly thank the anonymous referees for helping improve the manuscript from its original form.

[46] Arthur Richmond thanks Lennard A. Fisk, Thomas E. Holzer, and Richard Woo for their assistance in evaluating this paper.

## References

- Axford, W. I. (1977), The three-dimensional structure of the interplanetary medium, in *Study of Traveling Interplanetary Phenomena*, edited by M. A. Schea, D. F. Smart, and S.-T. Wu, p. 145, Springer, New York.
- Axford, W. I., and J. F. McKenzie (1997), The solar wind, in *Cosmic Winds in the Heliosphere*, edited by J. R. Jokipii, C. P. Sonett, and M. S. Giampapa, p. 31, Univ. of Ariz. Press, Tucson.
- Chiuderi Drago, F., E. Landi, A. Fludra, and A. Kerdraon (1999), EUV and radio observations of an equatorial coronal hole, *Astron. Astrophys.*, **348**, 261–270.
- Cranmer, S. R. (2002), Solar wind acceleration in coronal holes, *Eur. Space Agency Spec. Publ., ESA-SP 508*, 361–366.
- Deforest, C. E., J. T. Hoeksema, J. B. Gurman, B. J. Thompson, S. P. Plunkett, R. Howard, R. C. Harrison, and D. M. Hassler (1997), Polar plume anatomy: Results of a coordinated observation, *Sol. Phys.*, **175**, 393–410.
- Delaboudiniere, J.-P., et al. (1995), EIT: Extreme-Ultraviolet Imaging Telescope for the SOHO mission, *Sol. Phys.*, **162**, 291–312.
- Domingo, V., B. Fleck, and A. I. Poland (1995), SOHO: The Solar and Heliospheric Observatory, *Sol. Phys.*, **162**, 1.
- Doschek, G. A., U. Feldman, M. E. VanHoosier, and J.-D. F. Bartoe (1976), The emission-line spectrum above the limb of the quiet sun - 1175–1940 Å, *Astrophys. J. Suppl. Ser.*, **31**, 417–443.
- Doschek, G. A., H. P. Warren, J. M. Laming, J. T. Mariska, K. Wilhelm, P. Lemaire, U. Schühle, and T. G. Moran (1997), Electron densities in the solar polar coronal holes from density sensitive line ratios of Si VIII and Si X, *Astrophys. J.*, **482**, L109.
- Doschek, G. A., M. J. Laming, U. Feldman, K. Wilhelm, P. Lemaire, U. Schühle, and D. M. Hassler (1998), The Si/Ne abundance ratio in polar coronal hole and quiet-sun coronal regions, *Astrophys. J.*, **504**, 573–587.
- Doschek, G. A., U. Feldman, J. M. Laming, U. Schühle, and K. Wilhelm (2001), Properties of solar polar coronal hole plasmas observed above the limb, *Astrophys. J.*, **546**, 559–568.
- Dwivedi, B. N., A. Mohan, and K. Wilhelm (2000), On the electron temperatures, densities and hot ions in coronal hole plasma observed by SUMER on SOHO, *Adv. Space Res.*, **25**, 1751–1756.
- Endeve, E., E. Leer, and T. E. Holzer (2003), Two-dimensional magnetohydrodynamic models of the solar corona: Mass loss from the streamer belt, *Astrophys. J.*, **589**, 1040–1053.
- Feldman, U. (1983), On the unresolved fine structures of the solar atmosphere in the 30,000–200,000 K temperature region, *Astrophys. J.*, **275**, 367–373.
- Feldman, U. (1987), On the unresolved fine structures of the solar atmosphere. II - The temperature region 200,000–500,000 K, *Astrophys. J.*, **320**, 426–429.
- Feldman, U. (1998), FIP effect in the solar upper atmosphere: Spectroscopic results, *Space Sci. Rev.*, **85**, 227–240.
- Feldman, U., and K. G. Widing (1993), Elemental abundances in the upper solar atmosphere of quiet and coronal hole regions (Te is approximately equal to  $4.3 \times 10^5$  K), *Astrophys. J.*, **414**, 381–388.
- Feldman, U., G. A. Doschek, M. E. VanHoosier, and J. D. Purcell (1976), The emission-line spectrum above the limb of a solar coronal hole - 1175–1940 Å, *Astrophys. J. Suppl. Ser.*, **31**, 445–466.
- Feldman, U., U. Schühle, K. G. Widing, and J. M. Laming (1998), Coronal composition above the solar equator and the North Pole as determined from spectra acquired by the SUMER instrument on SOHO, *Astrophys. J.*, **505**, 999–1006.
- Feldman, U., G. A. Doschek, U. Schühle, and K. Wilhelm (1999a), Properties of quiet-sun coronal plasmas at distances of  $1.03 \leq R_{solar} \leq 1.50$  along the solar equatorial plane, *Astrophys. J.*, **518**, 500–507.
- Feldman, U., K. G. Widing, and H. P. Warren (1999b), Morphology of the quiet solar upper atmosphere in the  $4 \times 10^4 \leq T_e \leq 1.4 \times 10^6$  K temperature regime, *Astrophys. J.*, **522**, 1133–1147.
- Feldman, U., I. E. Dammasch, and K. Wilhelm (2000), The morphology of the solar upper atmosphere during the sunspot minimum, *Space Sci. Rev.*, **93**, 411–472.

- Feldman, U., I. E. Dammasch, K. Wilhelm, P. Lemaire, and D. M. Hassler (2003), Images of the solar upper atmosphere from SUMER on SOHO, *Eur. Space Agency Spec. Publ., ESA-SP 1274*, 1–209.
- Fisk, L. A. (2003), Acceleration of the solar wind as a result of the reconnection of open magnetic flux with coronal loops, *J. Geophys. Res.*, **108**(A4), 1157, doi:10.1029/2002JA009284.
- Fisk, L. A., and N. A. Schwadron (2001), The behavior of the open magnetic field of the sun, *Astrophys. J.*, **560**, 425–438.
- Fisk, L. A., T. H. Zurbuchen, and N. A. Schwadron (1999a), On the coronal magnetic field: Consequences of large-scale motions, *Astrophys. J.*, **521**, 868–877.
- Fisk, L. A., N. A. Schwadron, and T. H. Zurbuchen (1999b), Acceleration of the fast solar wind by the emergence of new magnetic flux, *J. Geophys. Res.*, **104**, 19,765–19,772.
- Gabriel, A. (1976), A magnetic model of the solar transition region, *Philos. Trans. R. Soc.*, **281**, 339–352.
- Gabriel, A. H., F. Bely-Dubau, and P. Lemaire (2003), The contribution of polar plumes to the fast solar wind, *Astrophys. J.*, **589**, 623–634.
- Geiss, J., et al. (1995), The southern high-speed stream – Results from the SWICS instrument on ULYSSES, *Science*, **268**, 1033–1036.
- Gloeckler, G., T. H. Zurbuchen, and J. Geiss (2003), Implications of the observed anticorrelation between solar wind speed and coronal electron temperature, *J. Geophys. Res.*, **108**(A4), 1158, doi:10.1029/2002JA009286.
- Handy, B. N., et al. (1999), The transition region and coronal explorer, *Sol. Phys.*, **187**, 229–260.
- Hollweg, J. V. (1986), Transition region, corona, and solar wind in coronal holes, *J. Geophys. Res.*, **91**, 4111–4125.
- Isenberg, P. A. (1989), *Geomagnetism*, vol. 3, Elsevier, New York.
- Kohl, J. L., et al. (1998), UVCS/SOHO empirical determinations of anisotropic velocity distributions in the solar corona, *Astrophys. J. Lett.*, **501**, 127–131.
- Kohl, J. L., S. Fineschi, R. Esser, A. Ciaravella, S. R. Cranmer, L. D. Gardner, R. Suleiman, G. Noci, and A. Modigliani (1999), UVCS/SOHO observations of spectral line profiles in polar coronal holes, *Space Sci. Rev.*, **87**, 233–236.
- Krieger, A. S., A. F. Timothy, and E. C. Roelof (1973), A coronal hole and its identification as the source of a high velocity solar wind stream, *Sol. Phys.*, **29**, 505.
- Laming, J. M., U. Feldman, J. J. Drake, and P. Lemaire (1999), The off-limb behavior of the first ionization potential effect in  $T \geq 5 \times 10^5$  K solar plasmas, *Astrophys. J.*, **518**, 926–936.
- Landi, E., and U. Feldman (2003), Properties of solar plasmas near solar maximum above two quiet region at distances of  $1.02\text{--}1.34 R_\odot$ , *Astrophys. J.*, **592**, 607–619.
- Li, X., S. R. Habbal, J. V. Hollweg, and R. Esser (1999), Heating and cooling of protons by turbulence-driven ion cyclotron waves in the fast solar wind, *J. Geophys. Res.*, **104**, 2521–2536.
- Lie-Svendsen, O., E. Leer, and V. H. Hansteen (2001), A 16-moment solar wind model: From the chromosphere to 1 AU, *J. Geophys. Res.*, **106**, 8217–8232.
- McComas, D. J., B. L. Barraclough, H. O. Funsten, J. T. Gosling, E. Santiago-Munoz, R. M. Skoug, B. E. Goldstein, M. Neugebauer, P. Riley, and A. Balogh (2000), Solar wind observations over Ulysses' first full polar orbit, *J. Geophys. Res.*, **105**, 10,419–10,434.
- Nolte, J. T., A. S. Krieger, E. C. Roelof, and R. E. Gold (1977), High coronal structure of high velocity solar wind stream sources, *Sol. Phys.*, **51**, 459–471.
- Olsen, E. L., E. Leer, and O. Lie-Svendsen (1998), An eight-moment model parameter study of the solar wind: Dependence on variations in coronal heating, *Astron. Astrophys.*, **338**, 747–755.
- Phillips, J. L., et al. (1995), ULYSSES solar wind plasma observations at high southerly latitudes, *Science*, **268**, 1030–1033.
- Schrijver, C. J., A. M. Title, A. A. van Ballegooijen, H. J. Hagenaar, and R. A. Shine (1997), Sustaining the quiet photospheric network: The balance of flux emergence, fragmentation, merging, and cancellation, *Astrophys. J.*, **487**, 424–436.
- Schrijver, C. J., A. M. Title, K. L. Harvey, N. R. Sheeley Jr., G. H. J. van den Oord, R. A. Shine, T. D. Tarbell, and N. E. Hurlburt (1998), Large-scale coronal heating by the small-scale magnetic field of the Sun, *Nature*, **394**, 152.
- Schwadron, N. A., and D. J. McComas (2003), Solar wind scaling law, *Astrophys. J.*, **599**, 1395–1403.
- Schwadron, N. A., L. A. Fisk, and T. H. Zurbuchen (1999), Elemental fractionation in the slow solar wind, *Astrophys. J.*, **521**, 859–867.
- Schwenn, R., et al. (1997), First view of the extended green-line emission corona at solar activity minimum using the Lasco-C1 coronagraph on SOHO, *Sol. Phys.*, **175**, 667–684.
- Sheeley, N. R., Jr. (1995), A volcanic origin for high-FIP material in the solar atmosphere, *Astrophys. J.*, **440**, 884.
- Teriaca, L., G. Poletto, M. Romoli, and D. A. Biesecker (2003), The nascent solar wind: Origin and acceleration, *Astrophys. J.*, **588**, 566.
- Tu, C.-Y., E. Marsch, K. Wilhelm, and W. Curdt (1997), Ion temperatures in a solar polar coronal hole observed by SUMER on SOHO, *Astrophys. J.*, **503**, 475.
- Usmanov, A. V., M. L. Goldstein, M. L. G. Besser, and J. M. Fritz (2000), A global MHD solar wind model with WKB Alfvén waves: Comparison with Ulysses data, *J. Geophys. Res.*, **105**, 12,675–12,696.
- von Steiger, R., N. A. Schwadron, S. Hefti, L. A. Fisk, J. Geiss, G. Gloeckler, B. Wilken, R. F. Wimmer-Schweingruber, and T. H. Zurbuchen (2000), Composition of quasi-stationary solar wind flows from Ulysses/Solar Wind Ion Composition Spectrometer, *J. Geophys. Res.*, **105**, 27,217–27,238.
- Wang, Y.-M., and N. R. Sheeley Jr. (2003), The solar wind and its magnetic sources at sunspot maximum, *Astrophys. J.*, **587**, 818–822.
- Warren, H. P. (1999), Measuring the physical properties of the solar corona: Results from SUMER/SOHO and TRACE, *Sol. Phys.*, **190**, 363–377.
- Widing, K. G. (1997), Emerging active regions on the sun and the photospheric abundance of neon, *Astrophys. J.*, **480**, 400–405.
- Widing, K. G., and U. Feldman (1992), Elemental abundances and their variations in the upper solar atmosphere, in *Solar Wind Seven*, edited by E. Marsch and R. Schwenn, pp. 405–410, Elsevier, New York.
- Widing, K. G., and U. Feldman (2001), On the rate of abundance modifications versus time in active region plasmas, *Astrophys. J.*, **555**, 426–434.
- Widing, K. G., E. Landi, and U. Feldman (2005), Coronal element comparison observed by SOHO/SUMER in the quiet southeast and northwest limb regions at  $1.05 R_\odot$  above the solar disk, *Astrophys. J.*, in press.
- Wilhelm, K. (1999), The darkest regions of solar polar coronal holes observed by SUMER on SOHO, *Astrophys. Space Sci.*, **264**, 43–52.
- Wilhelm, K., et al. (1995), SUMER - Solar Ultraviolet Measurements of Emitted Radiation, *Sol. Phys.*, **162**, 189–231.
- Woo, R., and S. R. Habbal (2000), Connecting the Sun and the solar wind: Source regions of the fast wind observed in interplanetary space, *J. Geophys. Res.*, **105**, 12,667–12,674.
- Woo, R., S. R. Habbal, and U. Feldman (2004), Role of closed magnetic field in solar wind flow, *Astrophys. J.*, **612**, 1171–1174.
- Young, P. R., J. A. Klimchuk, and H. E. Mason (1999), Temperature and density in a polar plume - Measurements from CDS/SOHO, *Astron. Astrophys.*, **350**, 286–301.
- Zurbuchen, T. H., S. Hefti, L. A. Fisk, G. Gloeckler, and R. von Steiger (1999), The transition between fast and slow solar wind from composition data, *Space Sci. Rev.*, **87**, 353–356.
- Zurbuchen, T. H., L. A. Fisk, G. Gloeckler, and R. von Steiger (2002), The solar wind composition throughout the solar cycle: A continuum of dynamic states, *Geophys. Res. Lett.*, **29**(9), 1352, doi:10.1029/2001GL013946.

U. Feldman and E. Landi, E. O. Hulbert Center for Space Research, Naval Research Laboratory, Washington, DC 20375-5320, USA. (uri.feldman@nrl.navy.mil; landi@poppeo.nrl.navy.mil)

N. A. Schwadron, Southwest Research Institute, P.O. Drawer 28510, San Antonio, TX 78228, USA.